A HARD X-RAY TWO-RIBBON FLARE OBSERVED WITH *YOHKOH*/HXT

S. MASUDA[1], T. KOSUGI[2] and H. S. HUDSON[3]
[1]*Solar-Terrestrial Environment Laboratory, Nagoya University, 3-13, Honohara, Toyokawa, Aichi 442-8507, Japan*
[2]*Institute of Space and Astronautical Science, 3-1-1, Yoshinodai, Sagamihara, Kanagawa 229-8510, Japan*
[3]*Solar Physics Research Corporation, 3-1-1, Yoshinodai, Sagamihara, Kanagawa 229-8510, Japan*

(Received ; accepted)

Abstract. The *Yohkoh* hard X-ray telescope (HXT) observed hard X-rays from the impulsive phase of a long-duration event (LDE) occurring on 14 July 2000. The *Yohkoh* soft X-ray telescope (SXT) and other instruments observed a large arcade, with width and length ∼30 000 km and ∼120 000 km, respectively. In hard X-rays, for the first time, a two-ribbon structure was clearly observed in the energy range above 30 keV. This result suggests that electrons are in fact accelerated in the whole system of this arcade, not merely in a particular dominant loop. We analyzed the motions of bright kernels in the two hard X-ray ribbons in detail. Assuming these bright kernels to be footpoints of newly reconnected loops, we infer from their motions that the loops reconnecting early are highly sheared, while the loops reconnecting later are less sheared. We have also analyzed the hard X-ray spectra of the two ribbons independently. At the outer edge of a ribbon, the spectrum tends to be harder than that in the inner edge. This suggests that higher-energy electrons precipitate at the footpoints of outer loops and lower ones do at those of inner loops. We discuss what kind of model can support this tendency.

1. Introduction

In solar flares, the two-ribbon structure is well known from Hα observations. A two-ribbon flare occurring on 7 August 1972, observed clearly at the Big Bear Solar Observatory, provided a classical example of such a development in Hα; Zirin in his textbook states that 'After the maximum the double ribbons separate and elongate, the space between them being filled with loop prominences condensing from the hot coronal cloud' (Zirin, 1988). In order to explain such features, theoretical models were proposed by many authors (e.g., Sturrock, 1966; Hirayama, 1974; Kopp and Pneuman, 1976). In their models, the two-ribbon structure is interpreted as a series of footpoints of coronal arcade loops which are created by successive magnetic reconnections taking place higher and higher above the arcade.

A two-ribbon flare structure has never been clearly observed in hard X-rays, although hard X-rays are emitted by high-energy electrons precipitating into the footpoints of flare loops. Usually we observe two or more point-like compact sources in hard X-rays during flares, even flares for which an Hα two-ribbon

Solar Physics **204:** 57–69, 2001.

structure is observed (Hoyng *et al.*, 1981; Sakao *et al.*, 1992). A statistical study was achieved by Sakao (1994), using the hard X-ray imaging data taken with the HXT (Kosugi *et al.*, 1991) on board *Yohkoh* (Ogawara *et al.*, 1991). According to his analysis of 28 flares selected with a criterion only on the hard X-ray flux, 39% (11/28) of the events showed a 'double source' structure. This structure was the most frequent type. The fractions of 'single source' and 'multiple source' flares were 29% and 32%, respectively. Incorporating other observational results, Sakao inferred that the double-source structure corresponded to the two footpoints of a flare loop, and that it is a fundamental structure in an energy range above 30 keV (Sakao, 1994). Although the Sakao sample did not distinguish two-ribbon flares in Hα from simple ones, it is certain that double footpoint sources, rather than ribbons, are usually observed in hard X-rays. This is a significant difference with Hα. Note that, of course, the Hα intensity depends on not only non-thermal electrons but also thermal conduction from the corona (e.g., Canfield, Gunkler, and Ricchiazzi, 1984; Gunkler *et al.*, 1984). Does particle acceleration take place efficiently only in some special magnetic field lines, or over a wide volume as suggested by the Hα ribbons and soft X-ray arcade structures? Or is this distinction due merely to the limited dynamic range of the HXT images?

Yohkoh/HXT has now clearly observed a two-ribbon flare in hard X-rays. The flare occurred on 14 July 2000, with nearly ideal properties (size, brightness, duration) for resolving this question. The observational results are described in Sections 2 and 3. In Section 4, we summarize both sets of results and discuss them.

2. Two-Ribbon Structure in Hard X-Rays

2.1. Overview

An X5.7 flare occurred on 14 July 2000. The *Yohkoh* satellite observed an early phase ($\sim$10:11–10:13 UT) and much of the extended impulsive phase of this flare. In soft X-rays, a large arcade structure is observed with the *Yohkoh* soft X-ray telescope SXT (Tsuneta *et al.*, 1991); the arcade's width and length were $\sim$30 000 km and $\sim$120 000 km, respectively. The western half of the arcade was almost exactly aligned in the E–W direction, and the eastern half in the NE–SW direction. The arcade brightened first in the west and then the brightening moved to the east. Figure 1 shows the hard X-ray time profiles observed with HXT. In the L-band (14–23 keV), the flux reaches its peak after a gap in the *Yohkoh* observations. Since we do not have other hard X-ray observations during the *Yohkoh* data gap, we know little about the flare behavior at high energies then. However, since there is no prominent mm-wave peak during the unobserved period (Magun, 2001), we are sure that *Yohkoh* did not miss the most energetic hard X-ray spike. After the *Yohkoh* data gap, there are two main spikes at higher energies. One spike starts just after the gap and reaches its peak at about 10:22 UT. In the second one, the hard

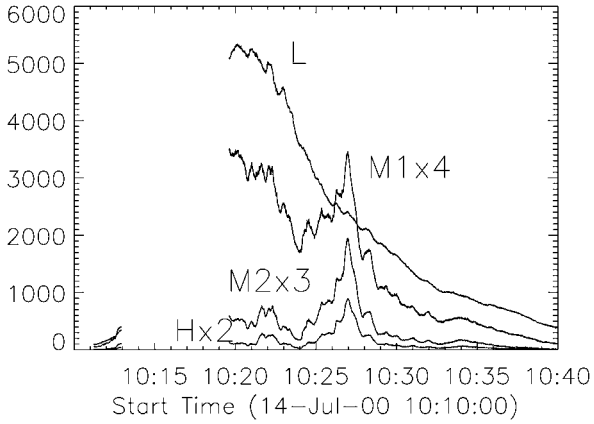

Figure 1. Hard X-ray time profiles observed with *Yohkoh*/HXT. The four HXT energy bands (the so-called L-, M1-, M2-, and H-bands) cover the energy ranges 14−23, 23−33, 33−53, and 53−93 keV, respectively. Units on the vertical axis are counts s^{-1} sc^{-1}, the total counting rate divided by the number (64) of subcollimators. There are no data from 10:13 UT to 10:19 UT.

X-ray flux increases at ∼10:24 UT, reaches a peak at ∼10:27 UT, and returns to its previous level at ∼10:30 UT. Since this flare shows completely different signatures in these two spikes, we distinguish them by the names S1 and S2, respectively. In this section and the next, we describe the observational results during S1 and S2 separately.

Figure 2 shows hard X-ray images in the four HXT energy bands during S1. These are snapshots synthesized with long integration times in order to gain image quality. When we discuss the temporal evolution, we use another data set synthesized with shorter integration times.

We find that a two-ribbon structure clearly appears in the energy ranges covered by the M2- (33−53 keV) and H-bands (53−93 keV). This is the first observation of such a two-ribbon structure in hard X-rays, although HXT has observed more than 2000 flares since *Yohkoh* was launched in 1991. This initial two-ribbon structure corresponds to a series of footpoints of the western part of the whole arcade observed with *Yohkoh*/SXT and with TRACE.

In the L-band, a diffuse single source is observed. It is located between the two ribbons observed in the higher-energy bands. The center position of this source fits within the brightest regions seen in soft X-rays well (Figure 2). The hard X-ray source also covers a high-temperature region seen in the temperature map derived from soft X-ray images taken with two different filters (Figure 2). This hard X-ray source has a soft spectrum and shows a gradual temporal variation. The count-rate ratio between M1- and L-bands of the gradual component is about 0.15 during this period; this would normally correspond to a high-temperature thermal spectrum. We infer that the arcade probably contains hot thermal plasma located near the ridge of the arcade loops. The hard X-ray images in the M1-band (23−33 keV) are complicated, because in this energy range, both spatial components (the two-

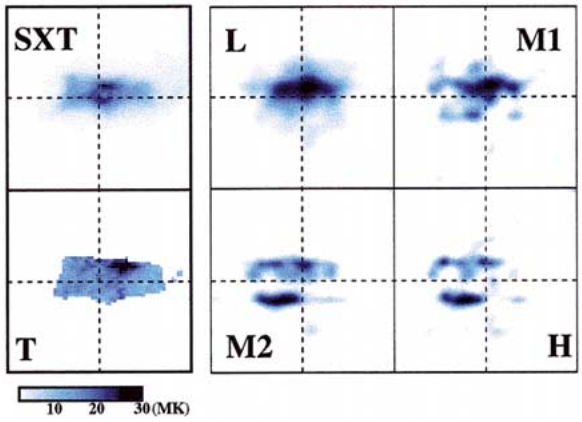

Figure 2. Soft X-ray image, temperature map, and hard X-ray images in the four HXT energy bands. The *upper left panel* shows a soft X-ray image taken with SXT/Be filter at 10:22:21 UT. The *lower left panel* is a temperature map derived from two soft X-ray images taken with different (Be and thick Al) filters at 10:22:21 UT and 10:22:19 UT, respectively. The *right four panels* show hard X-ray images in the four HXT energy bands. Counts were accumulated from 10:22:17 UT to 10:22:44 UT to synthesize these images. The field of view of each panel is $157'' \times 157''$.

ribbon structure and the ridge of the arcade) are present. With increasing energy, the hard X-ray emitting region gradually changes from a large diffuse source at the ridge of soft X-ray arcade, to a two-ribbon structure at the loop footpoints. These characteristics are analogous to the pattern found for impulsive flares observed with HXT, if we identify the two ribbons and the ridge of the arcade with the double footpoint sources and the loop-top source, respectively (Masuda *et al.*, 1994, 1995; Alexander and Metcalf, 1997; Masuda and Sato, 1998).

2.2. Motion of kernels inside the ribbons

Hα ribbons typically do not show uniform brightness. Usually several bright patches, the so-called kernels, are observed within one ribbon. In our first opportunity, we also find bright compact kernels in hard X-rays to occur along a ribbon. We have examined the evolution of these bright kernels during spike S1. As mentioned before, the two-ribbon structure is clearly observed during this period. Figure 3 shows the evolution of the hard X-ray sources during S1. In each panel, we connect the most intense source in the northern ribbon and the most intense source in the southern ribbon by a thick line. The angle between this line and the normal to the magnetic neutral line, the so-called shear angle, seems to decrease gradually. Especially at the early and late phases in Figure 3, however, it is difficult to determine the magnetic connectivity between the northern and southern kernels by this simple means. Here, we use only the spike period 10:21:10 UT–10:22:35 UT, to discuss the change of the shear angle. During this period there is only a single intense kernel in each ribbon, and these two kernels show quite similar time profiles as

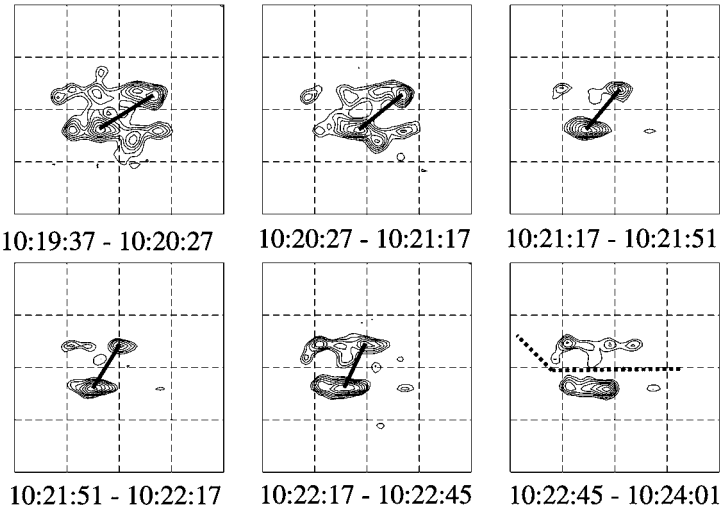

Figure 3. H-band images during the first spike (10:19–10:24 UT). The field of view of each panel is $157'' \times 157''$. The contour levels are 70.7, 50.0, 35.4, 25.0, 17.7, 12.5, and 8.8% of the peak intensity for each panel. A *thick line* connects the most intense kernels in the two-ribbon structure. In the final panel, a simplified magnetic neutral line is shown by a *thick dotted line* according to the SOHO/MDI observations.

illustrated in Figure 4. These properties strongly suggest that we have identified the magnetic connectivities of the loop footpoints correctly. Figure 4 shows the motion of these two kernels during the spike. We use a series of images in the M2-band instead of the H-band in order to achieve higher time resolution; the M2-band images are similar to those in the H-band (cf., Figure 2). At 10:21:10 UT, the northern kernel is located about 22 000 km west of the southern kernel. The southern kernel moves to the west and the E–W difference between the two kernels becomes only ∼14 000 km at about 10:22:35 UT. In the north–south direction, the northern kernel moves north the southern one moves south during this period, consistent with ribbon separation. The shear angle decreases during these motions.

The standard reconnection models do not make clear predictions for this behavior. They generally expect that the the inner (lower) magnetic fields reconnect first, and then the outer (higher) ones. In two dimensions the newly-reconnected loops would lie above the loops previously reconnected. The time profiles of the two sources we have selected seem to be similar within the time resolution (Figure 4). Assuming that this pair of hard X-ray sources corresponds to the two ends of a series of reconnected magnetic loops, this result suggests that the early, lower loops retain higher shear angles than the later, higher loops. Although we cannot say that all of the loops in this arcade have the same tendency, at least the magnetic loops related to the most important particle acceleration do behave in this manner. The evolution of the footpoint locations maps into the 3D coronal magnetic structure in ways that we do not fully understand at present.

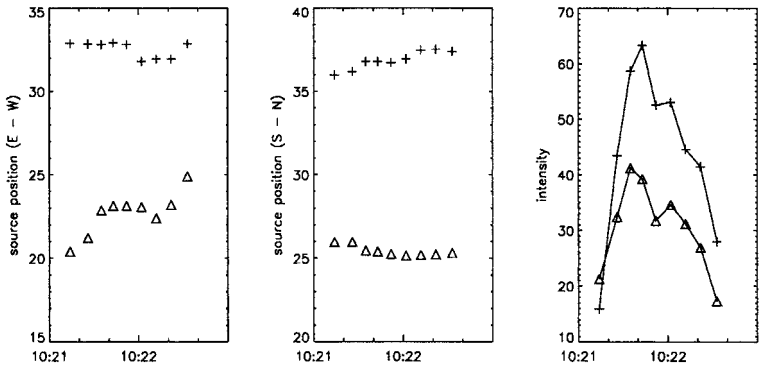

Figure 4. Left and center: Motion of the centroid of the most intense hard X-ray sources in the northern and southern ribbons. The *left panel* shows the motion along the east (*bottom*) – west (*top*) direction. The source in the northern ribbon (+) moves to the east, and the source in the southern ribbon (△) moves to the west. The *center panel* shows the motion along the south (*bottom*) – north (*top*) direction. The source in the northern ribbon moves to the north, and the source in the southern ribbon moves to the south. This means the two sources move outward from the magnetic neutral line. The unit of these panels is 2.46 arc sec, the same as the SXT CCD pixel size. *Right*: Time profiles of the most intense source in the northern (+) and the southern (△) ribbon. The unit of the vertical axis is cts s^{-1} cm^{-2}.

2.3. SPECTRAL CHARACTERISTICS

We have also investigated the hard X-ray spectral characteristics of the two-ribbon structure. Figure 5 show spectral-index maps in the three periods, which are the rising, peak, and decay phases of the spike S1. We derived these maps from the count ratio between M2- and H-band, assuming that the hard X-rays are emitted by thick-target bremsstrahlung (Brown, 1971). The number of photons in each map is ample to synthesize reliable images, and we conservatively used only those parts of the images whose intensity exceeded 10% of the maximum intensity of each map. Still there may be uncertainty in the small-scale structures and minor components in these maps. We discuss only the large-scale global structure here. The spectrum in the whole system shows a temporal evolution of the 'soft-hard-soft' pattern, as is typically observed in impulsive flares. In the rising and decay phase, the power-law index in most of the area is larger than 4. We find that the soft-hard-soft pattern extends globally, since the power-law index becomes smaller than 4 in most of emitting area at the peak time.

In the first panel of Figure 5, there is a region with a soft spectrum between the two ribbons. This region corresponds to the hard X-ray source observed in the lower energy bands. A super-hot thermal component ($T > 30$ MK) could contribute to the emission here; hot thermal emission can be seen in the Fe XXIV response of the TRACE 195 Å images. We note that the GOES temperature at this time is below 20 MK. We also find that the hard X-ray spectrum at the outer edge of the ribbons is harder than that at the inner part. The hardness of the spectrum gradually

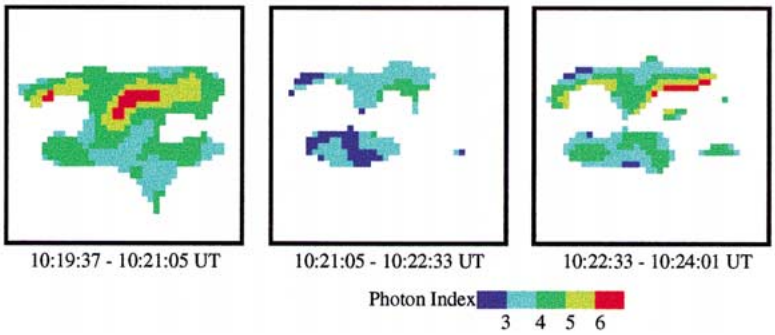

Figure 5. Spectral maps during the first spike (10:19–10:24 UT). First a count-ratio map is created from the M2- and H-band images synthesized with a common set of parameters. Assuming a single power-law spectrum at each point, we can then generate a spectrum map. A lower power-law index indicates a harder spectrum. The field of view of each map is $98'' \times 98''$.

changes across the ribbon width. This property is clear at the northern ribbon in the third panel. We discuss what this feature may mean in Section 4.

3. Hard X-Ray Sources during the Second Spike

In the previous section, we focused on the first half of the hard X-ray observations. This section describes the hard X-ray features after 10:24 UT. During spike S2, the hard X-ray emitting region completely moves to the eastern half of the whole arcade system in both the M2- and H-bands. It is as though a separate flare has begun to the east of the previous one. However, in the L-band, the hard X-ray images are still dominated by the region emitting during S1. Until at least 10:31 UT, the location of the L-band X-ray source does not change appreciably. This is as expected from the time profile (Figure 1). In the M1-band, we cannot get good images except at the time just around the peak during S2. We believe that this is because both the east and west regions contribute, so that the images become too large for a successful synthesis. At this time we presumably have the hot thermal component in the west, and new footpoint sources in the east. Here there is a very unusual feature in the time profiles (Figure 1). In the L-band, the gradual component, which had remained from S1, is dominant. Surprisingly the hard X-ray enhancement during S2 in the L-band seems to be less than 200 counts s^{-1} sc^{-1}, although the enhancement is greater than 500 counts s^{-1} sc^{-1} in the M1-band[1]. According to the HXT spectral response (Kosugi *et al.*, 1991), this certainly suggests that few lower-energy (< 23 keV) non-thermal electrons have been accelerated during S2, but the upper limit in the L-band lies below any count rates calculated in the framework of thick-target bremsstrahlung, given the

[1]The instrument-level unit of flux in HXT is counts per second per subcollimator, defined as 1/64 of the total counting rate because there are 64 subcollimators. This unit is close to counts cm^{-2} s^{-1}.

instrumental response function. We do not understand this behavior yet and hope to deal with it in detail in a future paper.

Figure 6 shows the evolution of hard X-ray sources in the M2-band during the second spike. A simplified magnetic neutral line is indicated in each panel. First an intense hard X-ray source appears at the east edge to the south of the neutral line, and another intense source appears at the west end in the north region. Both sources are located near the neutral line initially. A few hard X-ray sources then appear and disappear during the peak, but gradually the hard X-ray sources separate from the neutral line on both sides of the neutral line. Accompanying the separation, a decrease of the shear angle is again observed. In the previous section, we showed the motions of hard X-ray kernels within the two ribbons during S1. During S2, the same kinds of motions are observed although a perpendicular motion (increasing the separation) is more clear than that during the S1 interval. This separating motion is clearly observed in TRACE (cf., Fletcher and Hudson, 2001) and SXT images. In the TRACE 195 Å images, the two-ribbon structure appears in the eastern half of the whole arcade at about 10:24 UT, about the same time as the start of S2. The separation of the two ribbons continuously increases until about 10:40 UT.

4. Discussions and Conclusions

We have analyzed the hard X-ray imaging observations of the X-class flare of 14 July 2000. This flare provides us with several novel results for arcade-type solar flares, in the context of hard X-radiation, the flare emission most closely linked to the energy release of the impulsive phase. The observational results are summarized below and also discussed in the following subsections.

(1) For the first time, a two-ribbon structure has been clearly observed in the energy range above 30 keV. This result suggests that electrons are in fact accelerated in the whole system of an arcade, and not merely in a particular dominant loop.

(2) Two kinds of motion, parallel and vertical to the magnetic neutral line, are observed in the hard X-ray kernels within the ribbons. Assuming that pairs of hard X-ray sources correspond to the two ends of reconnected magnetic loops, this result suggests that the earlier reconnections lead to more highly sheared loops, with the latter less sheared. This kind of observation introduces a new way of studying the coronal field dynamics.

(3) The spectrum at the outer edges of the hard X-ray ribbons is harder than that at the inner part. The hardness of the spectrum gradually changes from the inner part to the outer part. This characteristics is clearly observed in the early and late phase during S1.

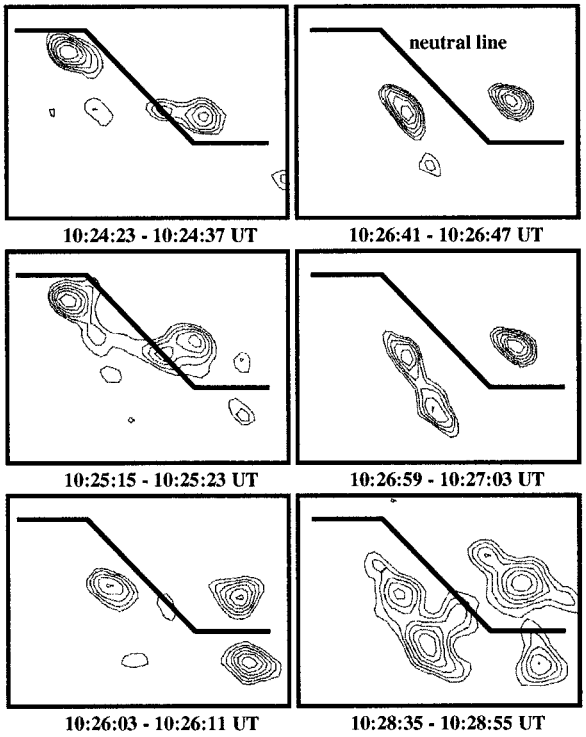

Figure 6. HXT M2-band images during the second spike (10:24–10:30 UT). The field of view of each panel is $120'' \times 90''$. The contour levels are 70.7, 50.0, 35.4, 25.0, 17.7, and 12.5% of the peak intensity of each image. The *thick line* in each panel indicates a simplified magnetic neutral line, referring to the SOHO/MDI observations.

4.1. TWO-RIBBON STRUCTURES IN HARD X-RAYS

Why have we never observed two-ribbon hard X-ray structures in large-scale solar flares, such as LDEs or arcade flares? Of course this flare may be unique, since it is our only good example thus far. However, it is more likely that the lack of other clear observations is due to limitations in the HXT imaging. The HXT (Kosugi *et al.*, 1991) is a hard X-ray imager of the Fourier-synthesis type. It has 64 modulation subcollimators, each measuring incident photon counts with a different spatial modulation. The intensity dynamic range of a synthesized HXT image typically does not exceed about 10 : 1. The limitation, we believe, comes from the restricted (u, v)-plane coverage of HXT and residual grid calibration errors (cf., Sato, Kosugi, and Makishima, 1999). This means that it is difficult to observe sources whose intensity is below 10% of the brightest peak. Larger, fainter, or more complicated sources may result in images with still lower dynamic range. As shown in this flare, the hard X-ray intensity in a ribbon is not uniform. Outstanding bright kernels are observed at various points within the ribbons, especially around the peak time. The two-ribbon structure is most clearly observed in the rising phase and the decay

phase of epoch S1. We thus attribute our success in detecting a clear two-ribbon structure to the uniformity of the arcade in this event.

To obtain high time resolution requires a large effective area to provide better counting statistics, plus a flat spectrum. In this event, we have many photons in the higher-energy bands, with an X-ray spectral index below $\gamma = 3$ during the S2 peak. However, most LDEs have relatively soft spectra (Masuda and Sato, 1998) and HXT does not detect enough photons to synthesize images in the higher bands. In order to synthesize an image which contains complex structure and large-scale sources, we need to reduce the error due to photon counting statistics. It is generally difficult to synthesize hard X-ray images in the rising phase (too brief) and the decay phase (too soft) because of poor photon counts. In this sense, the present event is unusual. Generally speaking, spatially larger events have longer time scales and softer spectra in the HXT energy range. For example, the 'global restructuring event' (large-scale arcade formation) reported by Tsuneta *et al.* (1992a), has huge spatial structure and lasts for about one day. HXT did not detect any excess photons from this event. In the case of the well-studied LDE of 21 February 1992 (Tsuneta *et al.*, 1992b), HXT detected only about 10 and 1 cts s^{-1} sc^{-1} in the L- and M1-bands at the peak time, and no significant fluxes were detected in the higher-energy bands. Hudson and McKenzie (2000) point out that even 'slow' LDEs (using the 21 February 1992 event as an example) do have hard X-ray fluences comparable to those of impulsive flares, but the counts spread out over longer time scales and may not exceed the detector background.

The observational limitations of HXT therefore have thus far made it impossible for us to detect hard X-ray ribbon structures in other LDEs. We believe that HESSI (Lin *et al.*, 2000) will provide new information about this topic because it will have a much wider dynamic range and a somewhat larger effective area.

4.2. Sheared arcade inferred from hard X-ray footpoint motions

The motions of the hard X-ray kernels in the ribbon were analyzed in detail. During the main spike time of S1, the kernels tended to appear in pairs, one in each ribbon; we interpret these as the two ends of a magnetic loop. The brightest kernel in the northern ribbon moves successively to the east and the north and *vice versa*. The apparent motion is in the sense of reducing the shear angle, as defined above. During S2 (Figure 6), the hard X-ray sources first appear at extreme elongations near the magnetic neutral line, then nearer together but at increasing separations from the neutral line. This would be consistent with the initially reconnected loops having high shear, and the subsequent reconnections resulting in less shear. We can infer such geometrical constraints on the coronal dynamics by assuming accelerated electrons precipitate along a reconnected loop, at both footpoints, as a result of energy release related to the formation of that loop.

Similar footpoint motions have also been observed in impulsive flares by Sakao (1999), but without the ribbon morphology. He noted a tendency for the footpoint

sources not to move apart (i.e., move in the direction of their separation), but most frequently to move nearly anti-parallel to each other and in directions perpendicular to their separation. These elongated trajectories might represent flare ribbons seen with poorer conditions than those in the 14 July 2000 event.

In the first panel of Figure 6, two intense sources are located near the east and west edges of the emission region during S2. In the later images, sources appear between these two sources. This implies that the global structure of the flaring region can be recognized from the outset, an observation which may be helpful in understanding the primary energy-release mechanism. Again similar results were reported by Sakao *et al.* (1992) in the 15 November 1991 flare. In the precursor phase of that event, the hard X-ray sources scatter across an area with a spatial extent greater than 40 000 km. In the impulsive and gradual phases, hard X-ray sources are located in a smaller area and do not exceed the outline of the hard X-rays sources found in the precursor phase.

Moore *et al.* (1997) proposed a magnetic field model for a large two-ribbon flare. In their scenario, the 'sheared core' field lines running under and out the ends of flare arcade reconnect initially. This creates longer loops whose footpoints are located at the two ends of the arcade, and shorter loops near the center of the arcade. At this time, all of the reconnected loops are still under the arcade. Subsequently the longer reconnected loop moves upward with the overlying fields as in the filament-eruption model of Hirayama (1974). Finally the main energy-release occurs via magnetic reconnection, throughout the whole system of the arcade. The two intense hard X-ray sources in the first panel of Figure 6 might correspond to the two ends of the longer loop reconnected initially in this model and within this model we can identify the shear-angle reduction as a progression in height, as well as time.

4.3. Particle acceleration in arcade flares

During interval S1 we observe that the hard X-ray spectrum at the outer edge of the ribbon is harder than that at the interior, and the hardness of the spectrum gradually changes across the ribbon width. During interval S2, this tendency is hardly observed since intense kernels are dominant and the ribbon structure is unclear. We suggest three possible interpretations here.

First there is a possibility of the contamination from the hot thermal component around the ridge of the arcade. From observations in the L- and M1-bands, we know there is hot plasma between the two ribbons. We cannot presently reject this possibility but expect that detailed modeling using multiple data sets, as for example in Warren *et al.* (1999), could do so.

The second is the difference of the average heights of the emitting region in the M2- and H-bands. Presumably hard X-ray footpoint sources are created by electron precipitation from a coronal source in the loop. Higher energy electrons can reach lower altitudes of the loop. Matsushita *et al.* (1992) reported differences of the average heights where hard X-rays are emitted in the M2- and H-bands. This flare

occurred almost at the center of the solar disk, so that the loops are observed from above. The outer edge of the ribbon might correspond to a lower altitude, if the coronal field lines inclined inwards towards the neutral line. The observed spectral tendency might imply this kind of geometry.

Finally, the spectral effect might be related to the acceleration mechanism. As we described before, the two-ribbon structure is clearly observed in both the rising and decay phases. The kernels (intense compact sources) within the ribbons have much shorter time scales. This could mean that the two-ribbon structure originates in the precipitation of *trapped* electrons with relatively longer time scales (Aschwanden *et al.*, 1996, 1997), and that the kernels result from direct precipitation. Assuming again that the inner loops result from early reconnection and the outer loops from later reconnection, relatively long-lived electrons precipitate at the inner footpoints at one observing moment. In this sense, higher-energy electrons precipitate quickly and lower-energy electrons are trapped for a longer time. Since this difference comes from the difference of the pitch-angle distribution, the acceleration should be field-aligned to explain this result.

Acknowledgements

We would like to express our acknowledgments to ISAS, NASA, SERC, and the *Yohkoh* team for their support to the mission. This work is partially supported by the Grant-in-Aid for Scientific Research of the Japan Society for the Promotion of Science No. 10640429 and 12640432. The work of HSH was supported by NASA under contract NAS8-40801.

References

Alexander, D. and Metcalf, T. R.: 1997, *Astrophys. J.* **489**, 442.
Aschwanden, M. J., Hudson, H. S., Kosugi, T., and Schwartz, R. A.: 1996, *Astrophys. J.* **464**, 985.
Aschwanden, M. J., Bynum, R. M., Kosugi, T., Hudson, H. S., and Schwartz, R. A.: 1997, *Astrophys. J.* **487**, 936.
Brown, J. C.: 1971, *Solar Phys.* **18**, 489.
Canfield, R. C., Gunkler, T. A., and Ricchiazzi, P. J.: 1984, *Astrophys. J.* **282**, 296.
Fletcher, L. and Hudson, H. S.: 2001, *Solar Phys.*, this issue.
Gunkler, T. A., Canfield, R. C., Acton, L. W., and Kiplinger, A. L.: 1984, *Astrophys. J.* **285**, 835.
Handy, B. N. *et al.*: 1999, *Solar Phys.* **187**, 229.
Hirayama, T.: 1974, *Solar Phys.*, **34**, 323.
Hoyng, P. *et al.*: 1981, *Astrophys. J.* **244**, L153.
Hudson, H. S. and McKenzie, D. E.: 2000, in R. Ramaty and N. Mandzhavidze (eds.), *High Energy Solar Physics – Anticipating HESSI, ASP Conference Series* **206**, 221.
Kopp, R. A. and Pneuman, G. W.: 1976, *Solar Phys.* **50**, 85.
Kosugi, T., Makishima, K., Murakami, T., Sakao, T., Dotani, T., Inda, M., Kai, K., Masuda, S., Nakajima, H., Ogawara, Y., Sawa, M., and Shibasaki, K.: 1991, *Solar Phys.* **136**, 17.

Lin, R. P. and the HESSI Team: 2000, *High Energy Solar Physics: Anticipating HESSI, ASP Conference Series* **206**, 1.

Magun, A.: 2001, private communication.

Masuda, S. and Sato J.: 1998, in E. Sagawa and M. Akioka (eds.), *Workshop on Solar Flares and Related Disturbances*, p. 52.

Masuda, S., Kosugi, T., Hara, H., Tsuneta, S., and Ogawara, Y.: 1994, *Nature* **371**, 495.

Masuda, S., Kosugi, T., Hara, H., Sakao, T., Shibata, K., and Tsuneta, S.: 1995, *Publ. Astron. Soc. Japan* **47**, 677.

Masuda, S., Kosugi, T., Sakao, T. and Sato, J.: 1998, in T. Watanabe, T. Kosugi, and A. C. Sterling (eds.), *Observational Plasma Astrophysics: Five Years of Yohkoh and Beyond*, p. 259.

Matsushita, K., Masuda, S., Kosugi, T., Inda, M., and Yaji, K.: 1992, *Publ. Astron. Soc. Japan* **44**, L89.

Moore, R. L., Schmieder, B., Hathaway, D. H., and Tarbell, T. D.: 1997, *Solar Phys.* **176**, 153.

Ogawara, Y., Takano, T., Kato, T., Kosugi, T., Tsuneta, S., Watanabe, T., Kondo, I., and Uchida, Y.: 1991, *Solar Phys.* **136**, 1.

Sakao, T.: 1994, Ph.D. Thesis, University of Tokyo.

Sakao, T.: 1999, *Proc. of the Nobeyama Symposium, Solar Physics with Radio Observations, NRO Report* **479**, 321.

Sakao, T., Kosugi, T., Masuda, S., Inda, M., Makishima, K., Canfield, R. C., Hudson, H. S., Metcalf, T. R., Wuelser, J.-P., Acton, L. W., and Ogawara, Y.: 1992, *Publ. Astron. Soc. Japan* **44**, L83.

Sato, J., Kosugi, T., and Makishima, M.: 1999, *Publ. Astron. Soc. Japan* **51**, 127.

Sturrock, P. A.: 1966, *Nature* **211**, 695.

Tsuneta, S., Acton, L., Bruner, M., Lemen, J., Brown, W., Caravalho, R., Catura, R., Freeland, S., Jurcevich, B., Morrison, M., Ogawara, Y., Hirayama, T., and Owens, J.: 1991, *Solar Phys.* **136**, 37.

Tsuneta, S., Takahashi, T., Acton, L. W., Bruner, M. E., Harvey, K. L., and Ogawara, Y.: 1992a, *Publ. Astron. Soc. Japan* **44**, L211.

Tsuneta, S., Hara, H., Shimizu, T., Acton, L. W., Strong, K. T., Hudson, H. S., and Ogawara, Y.: 1992b, *Publ. Astron. Soc. Japan* **44**, L63.

Warren, H. P., Bookbinder, J. A., Forbes, T. G., Golub, L., Hudson, H. S., Reeves, K., and Warshall, A.: 1999, *Astrophys. J.* **527**, L121.

Zirin, H.: 1988, *Astrophysics of the Sun*, Cambridge University Press, Cambridge.